

A Nonlinear Variational Method for Improved Quantification of Myocardial Blood Flow Using Dynamic H_2^{15}O PET

Martin Benning, Thomas Kösters, Frank Wübbeling, Klaus Schäfers, Martin Burger

Abstract— H_2^{15}O as a PET-tracer offers the opportunity to examine perfusion of blood into tissue non-invasively (cf. [1]). It features a short radioactive half-life (≈ 2 min.) and therefore adds a smaller radiation exposure to the patient in comparison to other tracers. The disadvantages arising from the short radioactive half-life are noisy, low-resolution reconstructions. Previous algorithms first reconstruct images from each dynamic H_2^{15}O dataset independently, e.g. via the standard EM-algorithm (cf. [2]) or FBP. Hence, temporal correlation is neglected. The myocardial blood flow (MBF) and other important parameters, like tissue fraction, arterial and venous spillover effects are computed subsequently from these reconstructed images. Our new method interprets the direct computation of parameters as a nonlinear inverse problem. This implies the need for inversion of a nonlinear operator $G(p)$ (with p denoting the parameters to compute), but allows to skip the process of generating noisy images. The process is schematically described in Figure 1. Therefore, our method takes into account the temporal correlation between the datasets, and not the correlation between noisy, low resolution images. The problem is transferred to a nonlinear parameter identification problem. Furthermore, regularization can be added to each parameter independently, assuring meaningful results.

I. INTRODUCTION

CARDIOVASCULAR diseases are the most common cause of death in many countries worldwide. Many cardiovascular diseases originate from a constriction of an artery due to a plaque formation in the vessel wall. If this plaque is increasing in size the flow of blood may be limited, which may then cause a myocardial disease. Moreover, if the plaque is unstable and detaches from the interior wall, it can cause a sudden heart attack or a stroke.

All these facts point out the importance of early medical diagnosis. Investigation of blood flow at an early stage could

Manuscript received November 14, 2008. This work was supported in part by SFB 656 MoBiI

Martin Benning is research assistant at the Institute for Computational and Applied Mathematics, University of Münster, 48149 Germany (telephone: +49-251-83-32756, e-mail: martin.benning@wwu.de).

Thomas Kösters is research assistant at the Institute for Computational and Applied Mathematics, University of Münster, 48149 Germany (telephone: +49-251-83-49309, e-mail: tkoes_01@math.uni-muenster.de).

Frank Wübbeling is PD at the Institute for Computational and Applied Mathematics, University of Münster, 48149 Germany (telephone: +49-251-83-33792, e-mail: frank.wuebbeling@math.uni-muenster.de).

Klaus Schäfers is PD at the Department of Nuclear Medicine, University Hospital of Münster, 48149 Germany (telephone: +49-251-83-49302, e-mail: schafkl@uni-muenster.de).

Martin Burger is professor at the Institute for Computational and Applied Mathematics, University of Münster, 48149 Germany (telephone: +49-251-83-33793, e-mail: martin.burger@wwu.de).

prevent latter heart attacks or other serious diseases. Examining the heart's blood flow and its amount of perfusable tissue under rest and stress conditions allows to gain further insight into future mischief.

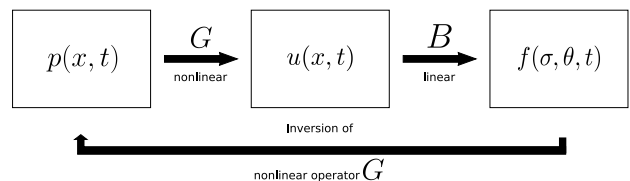


Fig. 1. Physiological parameters produce an image sequence u via a nonlinear operator G . These images are transformed to PET data f via a linear operator B . Inverting B and G allows to compute parameters from the PET data instead of the image sequence.

An alternative and complementary approach to catheterization is to examine the patient with PET (Positron Emission Tomography), which is a non-invasive nuclear imaging technique that allows to make physiological processes within the body visible. H_2^{15}O is injected into the patients body. The fact that H_2^{15}O is highly diffusive allows to monitor the perfusion of myocardial tissue. Via a physiological model, quantitative conclusions can be drawn on possible occlusion of coronary arteries.

In comparison to catheterization, MBF-examination via H_2^{15}O PET is not cumbersome and does not involve all the risks catheterization comes along with, like e.g. the risk for thrombosis, embolism or infections. Furthermore catheterization does not allow the distinction between a constricted or blocked vessel.

However, H_2^{15}O PET also has a big disadvantage. Due to a short half-time of H_2^{15}O (≈ 2 min) the patient's radiation exposure is pleasantly small, but unfortunately also most PET reconstructions are of very poor quality.

Nevertheless, state-of-the-art MBF-quantification methods compute MBF under the use of these low-quality PET reconstructions in order to draw conclusions of how well blood flows through the heart's vessels. The results allow quantitative estimates on MBF for a few regions of the heart only. The only stable estimate can be computed as the mean over the whole cardiovascular region.

In order to improve MBF-quantification we propose to compute the parameters right from the data (e.g. [3]). Our new method will be based on variational calculus and take into account the temporal correlation of the PET datasets, which is neglected in most state-of-the-art algorithms. We are going to

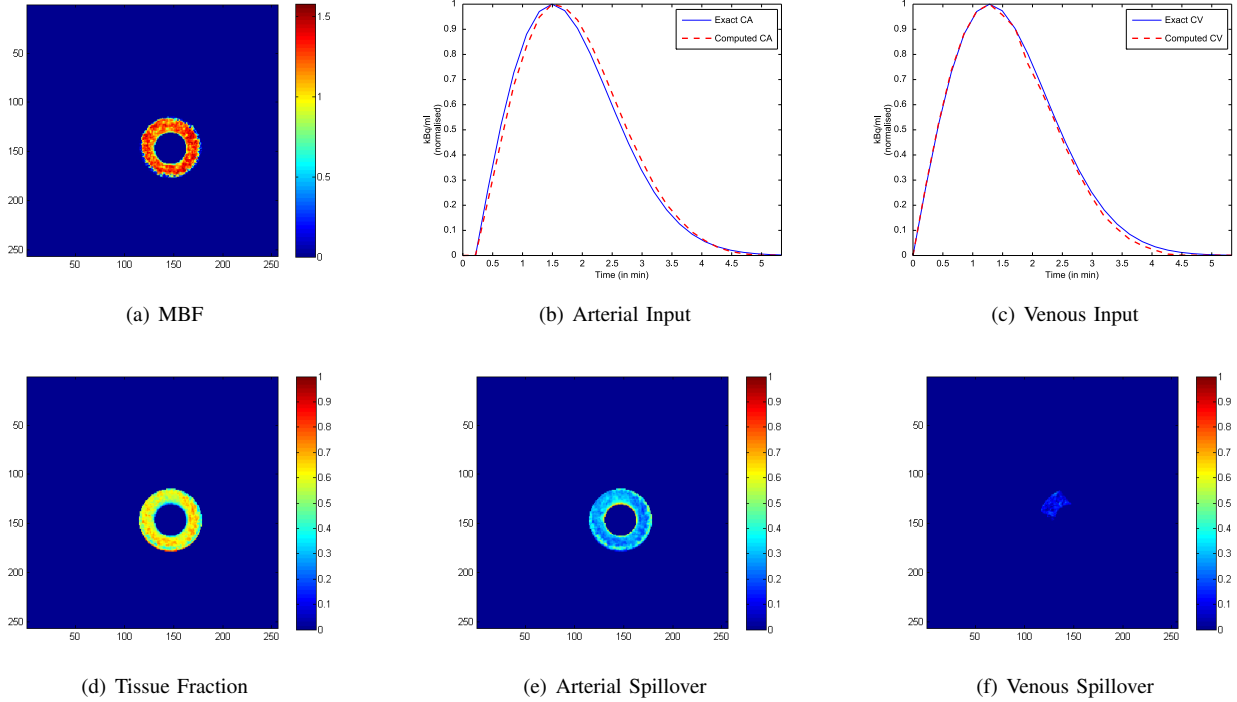


Fig. 2. Computational results of MBF quantification for the synthetic dataset described in Section IV-A1. In Figure 2(a) we can see the reconstruction of the MBF, which is in average close to the given value of $F = 1.248$ ml/min/mg. In Figure 2(b) the computed arterial input curve is compared with the set arterial input curve; Figure 2(c) shows the same for the venous input curve. The reconstructions in Figure 2(d), Figure 2(e) and Figure 2(f) show reconstructions of tissue fraction r and the arterial and venous spillover effects s_1 and s_2 , which are close to the given values, despite poor statistics.

develop a nonlinear mathematical model for the generation of PET data originating in physiological models for MBF. The inverse process then can be interpreted as the inversion of a nonlinear operator in order to obtain MBF from PET data. With this approach we compute reconstructions that do not neglect the temporal correlation among the different PET datasets over time and therefore compute better quantitative estimates of regional MBF.

II. THE INVERSE PROBLEM

With given PET sinogram data $f(\theta, y)$ the inverse problem of generating an image $u(x)$ from this data is to compute u from

$$\wp(Bu) = f. \quad (1)$$

The operator \wp denotes Poisson statistics of the data and B denotes the X-ray transform, defined via

$$(Bu)(\theta, y) = \int_{\mathbb{R}} u(y + s\theta) ds, \quad (2)$$

with $u \in L_2(\Omega)$, $\Omega \subset \mathbb{R}^n$, $\theta \in S^{n-1}$ and $y \in \theta^\perp$, which, in the case of two dimensions, is equivalent to the Radon transform. We want to mention that in equation (1) additive Gaussian noise is neglected. A solution approach for this inverse problem, taking into account that positrons are Poisson distributed, is

given via the minimization of the negative log-likelihood, i.e.

$$u \in \arg \min_{u \in L_2(\Omega)} \left\{ \int_{\Sigma} Bu - f \log(Bu) d\sigma(\theta, y) \right\}, \quad (3)$$

equivalently by minimizing the Kullback-Leibler functional

$$u \in \arg \min_{u \in L_2(\Omega)} \left\{ \int_{\Sigma} f \log \left(\frac{f}{Bu} \right) + Bu - f d\sigma(\theta, y) d\sigma(\theta, y) \right\}, \quad (4)$$

with $\Sigma \subset \mathcal{Q}$, and \mathcal{Q} being defined as

$$\mathcal{Q} := \{(\theta, y) \in S^{n-1} : y \in \theta^\perp\}. \quad (5)$$

Computing the Fréchet derivative of (3) or (4) with respect to u and setting one of them to zero yields the (formal) optimality condition

$$0 = B^*1 - B^* \left(\frac{f}{Bu} \right), \quad (6)$$

where B^* is the adjoint operator of B and 1 denotes the constant function taking only the value one. A computational solution of (6) can be obtained via the fixedpoint iteration

$$u_{k+\frac{1}{2}} = \frac{u_k}{B^*1} B^* \left(\frac{f}{Bu_k} \right), \quad (7)$$

known as the standard EM algorithm presented in [2].

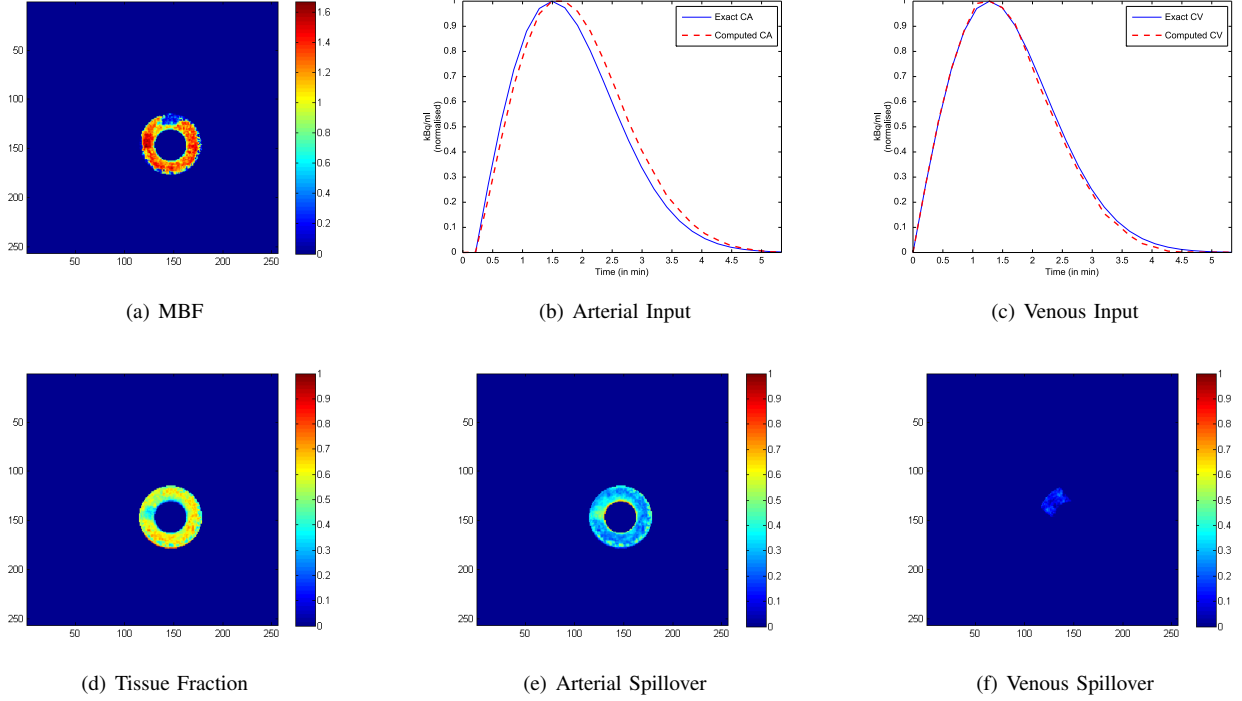


Fig. 3. Computational results of MBF quantification for the synthetic dataset described in Section IV-A2. In comparison to Figure 2 the MBF reconstruction perfectly indicates the area of low perfusion, while the region of higher perfusion in comparison to the uniform perfusion is smeared out.

A. The Inverse Problem of MBF Quantification

In comparison to (1) the quantification of MBF can be interpreted as a solution of the inverse problem of computing physiological parameters $p(x, t)$ from

$$\wp(BG(p)) = f, \quad (8)$$

with given sinogram data sampled over time, $f(\theta, y, t)$. Again, B denotes the X-ray transform, defined via

$$(Bu)(\theta, y, t) = \int_{\mathbb{R}} u(y + s\theta, t) ds, \quad (9)$$

with $u \in L_2(\Omega \times [0, T])$, $T \in \mathbb{R}_+$. The operator G is a nonlinear operator that produces an image sequence $u(x, t)$ from physiological parameters $p(x, t)$. A solution, with added regularization \mathcal{R} to p , can be given via

$$p \in \arg \min_{p \in \mathcal{P}} \{KL_T(f, BG(p)) + \mathcal{R}(p)\}, \quad (10)$$

with \mathcal{P} denoting the domain of parameters, and $KL_T(f, g)$ being the time-dependent Kullback-Leibler functional

$$KL_T(f, g) := \int_0^T \int_{\Sigma} f \log \left(\frac{f}{g} \right) + g - f d\sigma(\theta, y) dt. \quad (11)$$

A solution of (10) can be obtained by considering the saddle point problem

$$p \in \arg \min_{u, p} \max_{\mu} \{ \mathcal{L}(u, p; \mu) \}, \quad (12)$$

with the associated Lagrange multiplier

$$\mathcal{L}(u, p, \mu) = KL_T(f, Bu) + \mathcal{R}(p) + \langle G(p) - u, \mu \rangle_{L_2(\Omega \times [0, T])}. \quad (13)$$

Computing the partial Fréchet derivatives of (13) and setting them to zero yields

$$0 = \frac{\partial}{\partial u} \mathcal{L}(u, p; \mu) = B^*1 - B^* \left(\frac{f}{Bu} \right) - \mu, \quad (14)$$

$$0 = \frac{\partial}{\partial p} \mathcal{L}(u, p; \mu) = \mathcal{R}'(p) + G'(p)^* \mu, \quad (15)$$

$$0 = \frac{\partial}{\partial \mu} \mathcal{L}(u, p; \mu) = G(p) - u. \quad (16)$$

If we multiply (14) with $\frac{u}{B^*1}$ we obtain

$$0 = u - \frac{u}{B^*1} B^* \left(\frac{f}{Bu} \right) - \frac{u\mu}{B^*1}, \quad (17)$$

which we solve via the fixedpointiteration

$$0 = u_{k+1} - u_{k+\frac{1}{2}} - \frac{u_k \mu}{B^*1},$$

or equivalently by dividing this equation by u_k

$$0 = \frac{u_{k+1} - u_{k+\frac{1}{2}}}{u_k} - \frac{\mu}{B^*1}, \quad (18)$$

with $u_{k+\frac{1}{2}}$ being the standard EM algorithm as defined in (7), for every single timestep t independently. If we assume $B^*1 = 1$ equation (18) can be seen as the solution of the

variational problem

$$u_{k+1} \in \arg \min_{u \in L_2(\Omega \times [0, T])} \left\{ \frac{1}{2} \int_0^T \int_{\Omega} \frac{(u - u_{k+\frac{1}{2}})^2}{u_k} dx dt - \langle u, \mu \rangle_{L_2(\Omega \times [0, T])} \right\}. \quad (19)$$

If we insert the constraint (16) and replace u with $G(p)$ we obtain

$$p \in \arg \min_{p \in \mathcal{P}} \left\{ \frac{1}{2} \int_0^T \int_{\Omega} \frac{(G(p) - u_{k+\frac{1}{2}})^2}{u_k} dx dt - \langle G(p), \mu \rangle_{L_2(\Omega \times [0, T])} \right\}, \quad (20)$$

subject to $G(p) = u_{k+1}$, with \mathcal{P} denoting the domain of parameters. It is easy to see that the Fréchet derivative of $\langle G(p), \mu \rangle$ in p is simply $G'(p)^* \mu$. Therefore, by using (15), we can replace $-\langle G(p), \mu \rangle$ with $\mathcal{R}(p)$ to obtain the reduced problem

$$p \in \arg \min_{p \in \mathcal{P}} \left\{ \frac{1}{2} \int_0^T \int_{\Omega} \frac{(G(p) - u_{k+\frac{1}{2}})^2}{u_k} dx dt + \mathcal{R}(p) \right\}, \quad (21)$$

subject to $G(p) = u_{k+1}$. To solve (21) we consider the semi-discrete optimization problem

$$p \in \arg \min_{u, p} \max_q \{ \mathcal{L}_k(u, p; q) \} \quad (22)$$

with

$$\mathcal{L}_k(u, p; q) = \frac{1}{2} \int_0^T \int_{\Omega} \frac{(u - u_{k+\frac{1}{2}})^2}{u_k} dx dt + \frac{\mathcal{R}(p)}{B^* 1} + \int_0^T \int_{\Omega} (G(p) - u) q dx dt. \quad (23)$$

In order to compute the optimal set of parameters p , we need to compute the partial Fréchet derivatives of (23) and compute to their zeros. The equations for $\partial_u \mathcal{L}(u, p; q) = 0$ and $\partial_q \mathcal{L}(u, p; q) = 0$ can obviously be computed analytically, via

$$q = \frac{u - u_{k+\frac{1}{2}}}{u_k} \quad (24)$$

and

$$u = G(p). \quad (25)$$

Since there are numerous parameters contained in p and G is nonlinear, the optimality conditions for the parameters have to be solved iteratively. Before we discuss the computational solution in Section III we will discuss two basic models for the nonlinear operator G .

B. Models for nonlinear MBF Quantification

The operator G can simply be based on a physiological model, e.g. the well-known single-compartmental model

$$\frac{\partial C_{\mathcal{T}}}{\partial t}(x, t) = F(x) \left(C_{\mathcal{A}}(t) - \frac{C_{\mathcal{T}}(x, t)}{\lambda} \right), \quad (26)$$

respectively its associated integral equation

$$\mathbf{C}_{\mathcal{T}}(F, C_{\mathcal{A}})(x, t) = F(x) \int_0^t C_{\mathcal{A}}(\tau) e^{-\frac{F(x)}{\lambda}(t-\tau)} d\tau, \quad (27)$$

with F being the MBF, $C_{\mathcal{V}}$ denoting the arterial input curve and λ representing the partition coefficient (cf. [4]). A solution of this operator equation, denoted with $C_{\mathcal{T}}$ describes activity in tissue. A common modification of (27) is the introduction of arterial and venous spillover, i.e.

$$\mathbf{C}_{\text{PET}}(F, C_{\mathcal{A}}, C_{\mathcal{V}}, r, s_1, s_2)(x, t) = r(x) \mathbf{C}_{\mathcal{T}}(F, C_{\mathcal{A}})(x, t) + s_1(x) C_{\mathcal{A}}(t) + s_2(x) C_{\mathcal{V}}(t), \quad (28)$$

where r denotes the fraction of tissue-activity $C_{\mathcal{T}}$ and s_1 and s_2 represent the spillover effects of arterial ($C_{\mathcal{A}}$) and venous ($C_{\mathcal{V}}$) input curves per spatial compartment x (cf. [5]). The operator G can then be modeled as

$$G(F, C_{\mathcal{A}}, C_{\mathcal{V}}) = \mathbf{C}_{\mathcal{T}}(F, C_{\mathcal{A}})|_{\mathcal{T}} + C_{\mathcal{A}}|_{\mathcal{A}} + C_{\mathcal{V}}|_{\mathcal{V}} + u_{k+\frac{1}{2}}|_{\Omega \setminus \mathcal{H}}, \quad (29)$$

with \mathcal{T} denoting the cardiovascular region of myocardial tissue, \mathcal{A} representing the left ventricular region, \mathcal{V} denoting the right ventricular region and $\mathcal{H} = \mathcal{T} \cup \mathcal{A} \cup \mathcal{V}$, as in the case of (27). In the case of (28) we obtain

$$G(F, C_{\mathcal{A}}, C_{\mathcal{V}}, r, s_1, s_2) = (r \mathbf{C}_{\mathcal{T}}(F, C_{\mathcal{A}}) + s_1 C_{\mathcal{A}})|_{\mathcal{M}} + \mathbf{C}_{\text{PET}}(F, C_{\mathcal{A}}, C_{\mathcal{V}}, r, s_1, s_2)|_{\mathcal{S}} + C_{\mathcal{A}}|_{\mathcal{A}} + C_{\mathcal{V}}|_{\mathcal{V}} + u_{k+\frac{1}{2}}|_{\Omega \setminus \mathcal{H}}, \quad (30)$$

with \mathcal{S} denoting the septum region and \mathcal{M} the region of myocardium without septum, i.e. $\mathcal{T} = \mathcal{M} \cup \mathcal{S}$. In the case of (29) we have $p = (F, C_{\mathcal{A}}, C_{\mathcal{V}})$; in the case of (28) we have $p = (F, C_{\mathcal{A}}, C_{\mathcal{V}}, r, s_1, s_2)$ (if we want to compute all parameters from the data and do not have some parameters given a-priori).

If no or only rough information on segmentation of the cardiovascular region is known, but a-priori knowledge of the arterial and venous input functions is given, (30) can simply be modified to $G = \mathbf{C}_{\text{PET}}$ or $G = \mathbf{C}_{\text{PET}}|_{\mathcal{H}} + u_{k+\frac{1}{2}}|_{\Omega \setminus \mathcal{H}}$.

We note that both of these models allow the use of any precomputed a-priori information (e.g. precomputed input curves) without large modifications. This allows flexibility and guarantees less ill-posedness with more parameters given a-priori. Furthermore, operators can be modeled not just for MBF quantification but for other applications (such as radioligand receptor binding in the brain, cf. [6]).

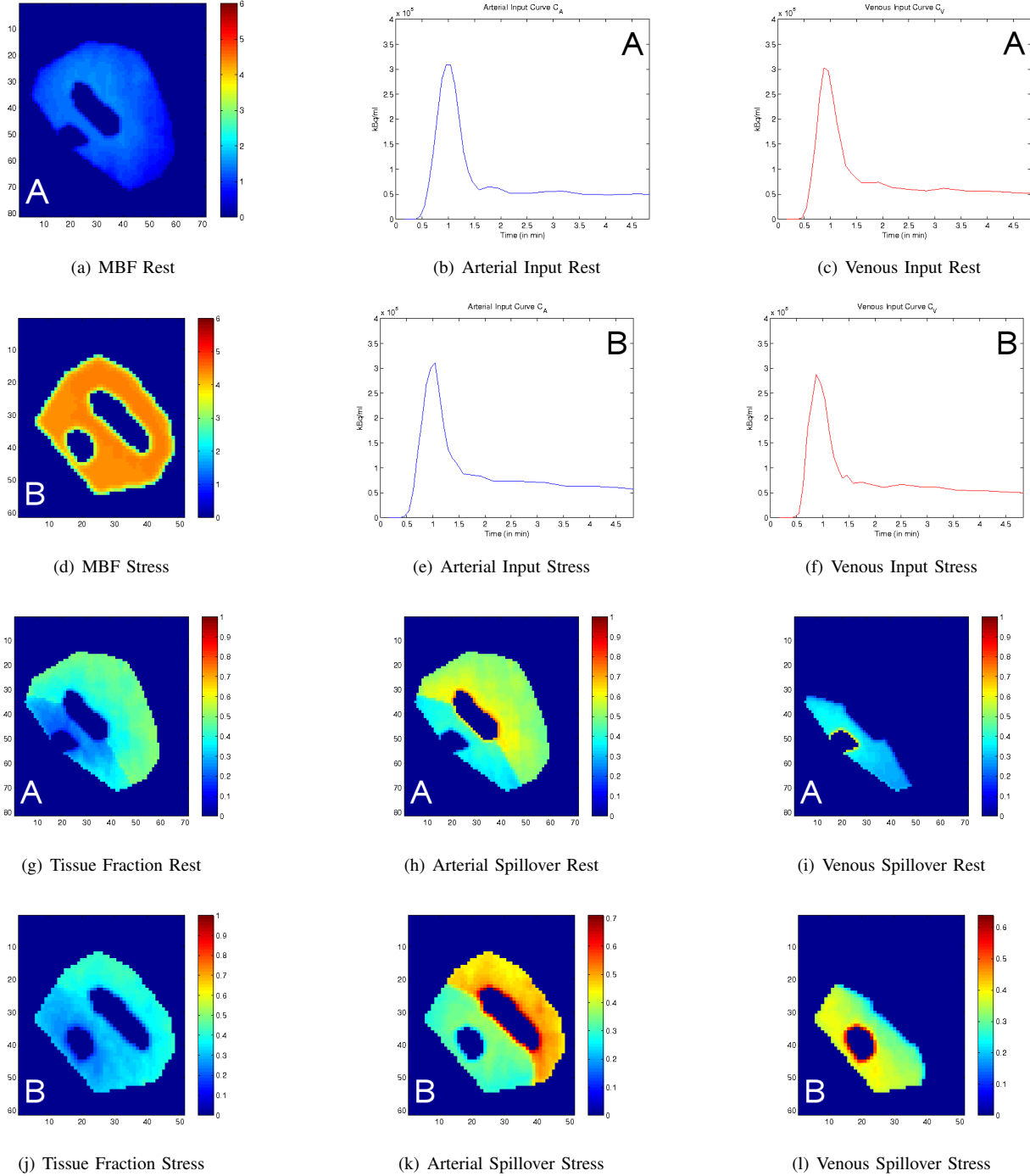


Fig. 4. Computational results that show exemplary reconstructions of real H_2^{15}O PET data, as described in Section IV-B. The reconstructions of MBF, arterial and venous input curves, tissue fraction and arterial and venous spillover are shown (from top left to bottom right). **A**: reconstructions under rest conditions. **B**: reconstructions under stress conditions.

III. NUMERICAL IMPLEMENTATION

The numerical computation of MBF quantification can be realized as a two-step procedure. First of all, an image sequence $u_{k+\frac{1}{2}}$ has to be computed via (7) from given PET data f for all times $t \in [0, T]$ independently (with an initial value $u_0(x, t) > 0$ for all $(x, t) \in \Omega \times [0, T]$).

The second step is to compute the optimal vector of parameters p that solve (22). If we assume p to contain l parameters,

i.e. $p = (p^i)_{i=\{1, \dots, l\}}$, we can simply compute each parameter via a Landweber iteration

$$p_{j+1}^i = p_j^i - \tau \partial_{p^i} \mathcal{L}_k(u, p_j, q), \quad (31)$$

with τ being small and q and u satisfying $\partial_u \mathcal{L}_k(u, p_j, q) = 0$ and $\partial_q \mathcal{L}_k(u, p_j, q) = 0$, respectively. If we stop iterating after m iterations (e.g. if $\|p_m - p_{m-1}\| < \varepsilon$, for ε small), we obtain

u_{k+1} via

$$u_{k+1} = G(p_m) \quad (32)$$

We reinsert u_{k+1} into the EM algorithm to compute $u_{k+\frac{3}{2}}$ and so on. We obtain a computational scheme as presented in Figure 5.



Fig. 5. The computational scheme for computing physiological parameters from the PET data. These parameters are computed via a two-step procedure containing the standard EM algorithm and a parameter identification (PI) process.

We want to mention that the choice of the Landweber iteration for computing the gradient descent of each parameter is not essential, rather the simplest choice for iterating the parameters. Other iterative methods (e.g. Newton-type methods) will lead to faster convergence and will be investigated in the future.

IV. COMPUTATIONAL RESULTS

In this section we want to present computational results of our new method. For that sake we generated synthetic, two-dimensional PET data via a simple Monte Carlo simulation with very poor Poisson statistics, to simulate the circumstances of a real $H_2^{15}O$ PET scan. In Section IV-A we are going to present computational results from these synthetic data sets. In Section IV-B we will pass over to real, two-dimensional $H_2^{15}O$ PET data.

For regularization, we simply chose a squared H_1 regularization term, i.e.

$$\mathcal{R}(p) = \frac{\alpha}{2} \|p\|_{H_1}^2, \quad (33)$$

or, if a-priori knowledge p^* is given (e.g. in terms of average values),

$$\mathcal{R}(p) = \frac{\alpha}{2} \|p - p^*\|_{H_1}^2, \quad (34)$$

with $\alpha > 0$, and additional regularization to tissue and spillover effects, as described in [7, Section 4.7.3], is added. Furthermore, all computations have been done based on the model (30).

A. Artificial Data

We want to present computational results for two synthetic data examples as introduced in [7, Chapter 6].

1) *Dataset 1*: In [7, Section 6.1] we generated a very simple synthetic dataset with uniform tissue activity. The artificial values used to generate this dataset were $F = 1.248$ ml/min/mg, $r = 0.65$, $s_1 = 0.21$, $s_2 = 0.15$ and λ has been set to a fixed value of 0.96. Figure 2 shows the computed reconstructions F_{rec} , $C_{A\text{rec}}$, $C_{V\text{rec}}$, r_{rec} , $s_{1\text{rec}}$ and $s_{2\text{rec}}$, which are pretty close to the specified synthetic parameters F , C_A , C_V , r , s_1 and s_2 .

2) *Dataset 2*: In the second artificial data example introduced in [7, Section 6.2] we simply modified the synthetic data example of Section IV-A1 to include nonuniform tissue activity. We specified three areas of tissue. In the first area we set the MBF to $F = 0.2$ ml/min/mg, while we set it to $F = 5$ ml/min/mg in the second area. In the remaining third region of tissue the MBF is set to be $F = 1.248$ ml/min/mg, as in the first data example IV-A1. All other parameters remained the same as in the example of IV-A1. The reconstructions can be seen in Figure 3.

B. Real Data

For the real data computations PET data of a two-dimensional slice, containing the cardiovascular region, have been processed under rest and stress conditions. Since no a-priori knowledge was given we computed all parameters from this slice. For that reason we were in the need to do a rough segmentation, which we did manually, based on EM-TV reconstructions (cf. [8]) of all PET datasets over time of that particular slice. Given this rough segmentation, we used (30) as our model to compute the parameters F , C_A , C_V , r , s_1 and s_2 . These computational results can be seen in Figure 4.

V. CONCLUSIONS

We presented a new algorithm to quantify MBF that takes into account the temporal correlation between the PET data sets. The new method offers encouraging results although its analysis is at the very beginning. There is a wide scope for improvements and extensions, such as full 4D PET or different physiological models, just to mention a few. For more details on MBF quantification as a nonlinear inverse problem we may suggest [7].

REFERENCES

- [1] K. P. Schäfers, T. J. Spinks, P. G. Camici, P. M. Bloomfield, C. G. Rhodes, M. P. Law, C. S. R. Baker, and O. Rimoldi, "Absolute Quantification of Myocardial Blood Flow with $H_2^{15}O$ and 3-Dimensional PET: An Experimental Validation," *Journal of Nuclear Medicine Vol.*, vol. 43, pp. 1031–1040.
- [2] A. P. Dempster, N. M. Laird, and D. B. Rubin, "Maximum Likelihood from Incomplete Data via the EM Algorithm," 1977.
- [3] M. E. Kamasak, C. A. Bouman, E. D. Morris, and K. Sauer, "Direct Reconstruction of Kinetic Parameter Images from Dynamic PET Data," *IEEE Transactions on Medical Imaging*, vol. 24, pp. 636–650, 2005.
- [4] S. R. Bergmann, K. A. Fox, and A. L. Rand, "Quantification of Regional Myocardial Blood Flow in Vivo with $H_2^{15}O$," *Circulation*, vol. 70, pp. 724–733, 1984.
- [5] H. Iida, I. Kanno, A. Takahashi, S. Miura, M. Murakami, K. Takahashi, Y. Ono, F. Shishido, A. Inugami, and N. Tomura, "Measurement of Absolute Myocardial Blood Flow with $H_2^{15}O$ and Dynamic Positron-Emission Tomography. Strategy for Quantification in Relation to the Partial-Volume Effect [published erratum appears in *Circulation* 1988 oct;78(4):1078]," *Circulation*, vol. 78, no. 1, pp. 104–115, 1988. [Online]. Available: <http://circ.ahajournals.org/cgi/content/abstract/78/1/104>
- [6] R. N. Gunn, A. A. Lammertsma, S. P. Hume, and V. J. Cunningham, "Parametric Imaging of Ligand-Receptor Binding in PET Using a Simplified Reference Region Model," *Neuroimage*, vol. 6, pp. 279–287, 1997.
- [7] M. Benning, "A Nonlinear Variational Method for Improved Quantification of Myocardial Blood Flow Using Dynamic $H_2^{15}O$ PET," 2008, Diploma Thesis. [Online]. Available: <http://wwwmath.uni-muenster.de/num/publications/2008/Ben08/diplomathesis.pdf>
- [8] A. Sawatzky, C. Brune, F. Wübbeling, T. Kösters, K. P. Schäfers, and M. Burger, "Accurate EM-TV Algorithm in PET with Low SNR," 2008, IEEE Nuclear Science Symposium and Medical Imaging Conference, MIC Poster II.